Materials Science-Poland, *Vol. 27*, *No. 3*, *2009*

Effect of milling time and addition of alumina powder on the structural properties and fracture surface of nanocrystalline Al

S.S. RAZAVI TOUSI, R.YAZDANI RAD*, E. SALAHI, M. RAZAVI

Ceramic Department, Materials and Energy Research Center, P.O. Box 31787/316, Karaj, Iran

The effects of milling time and the addition of alumina reinforcement on the structural evolution of Al matrix were investigated. By analysing the cross section of powder, cold welding mechanism for both monolithic and composite powders was studied. Results show that presence of the alumina powder has a marked effect on variation of apparent density, preferred orientation, impurity content and thus lattice parameter of Al by milling time. The reduction of the grain size to the nanometeric scale changes the fracture mechanism of Al particles completely, from dimpled into intergranular, though alumina addition does not seem to have notable influence on the fracture mechanism.

Key words: *ball milling; nanostructured materials; fracture surface*

1. Introduction

In order to predict the final properties of samples produced by ball milling, an accurate investigation into the structural evolution, dependent on the milling time, should be considered. With regard to the effect on the structural properties, addition of small amounts of ceramic phases into a ductile matrix has been studied in several works [1–6]. However, the addition of higher volume proportions (e.g., up to 20 wt. %) of ceramic phase has not been considered much up to now [7]. Fracture and welding are known to be the two major mechanisms affecting structural evolution during mechanical alloying (MA) [8]. For both brittle and ductile components, the systems do not reach the steady state as long as one of these mechanisms prevails [9]. Bearing this in mind, fracture and welding in monolithic Al and Al–Al_2O_3 systems will be studied.

Ceramic powder affects cold welding and fracture mechanism of the matrix. Thus, time necessary to reach the steady state, porosity and orientation of crystallites change in comparison with the monolithic ductile metal [2, 3].

*Corresponding author, e-mail: ryazdani5@gmail.com

As crystallite size is reduced to less than 100 nm, metals change from ductile to brittle [10]. Nevertheless, dimpled fracture surfaces have been observed in many nanocrystalline materials [11–15]. As will be discussed, in spite of the appearance of a fracture surface of nano-grained metals, cracks propagate along the grain boundaries (GBs) and the fracture surface is completely intergranular [16, 17].

2. Experimental

Monolithic Al powder (Merck, Art. No: 1056) and a mixture of Al–20 wt. % Al_2O_3 powder (Martinswerk, MR70, d_{50}: 0.5–0.8 μm) with 3 wt. % of stearic acid as the process control agent (PCA) were milled in a P5 planetary mill for various periods of time, up to 25 h. The milling atmosphere was Ar and the product sampling was performed in a glow box, to prevent oxidation. Samples were examined under an optical microscope (OM) and a Cambridge scanning electron microscope (SEM) operating at a voltage of 30 kV. A Philips CM 200 FEG transmission electron microscope (TEM) was used to investigate the grain size and dispersoids. The X ray diffraction (XRD) patterns were taken using a Siemens X ray diffractometer (30 kV and 25 mA).

Grain size changes during the milling stages were calculated by the Williamson –Hall method for at least three peaks [18]:

$$B\cos\theta = \frac{0.9\lambda}{D} + 2\eta\sin\theta \tag{1}$$

where B, λ, θ, D and η are FWHM, the wave length, peak position, crystallite size and lattice strain, respectively.

In order to minimize errors caused by aberration of 2θ variation, the Nelson–Riely method was used to calculate the lattice parameter of Al for at least three peaks, using Eq. (1) [19].

$$F(\theta) = 0.5\left(\frac{\cos^2\theta}{\sin^2\theta} + \frac{\cos^2\theta}{\theta}\right) \tag{2}$$

The minor errors caused by peak position displacement and peak shape deformation were reduced by the following procedure: peak position of each peak assigned to the middle of three $P_{x/y}$ with x/y equal to 0.6, 0.8 and 1, the final peak position was obtained by averaging these values. Full details of this method have been described elsewhere [20].

The powders were then pressed with an isostatic press (1 GPa) and sintered at 640 °C for 30 min. Fracture testing was carried out at a 3.3×10^{-2} (s^{-1}) strain rate at room temperature, and neither etching nor particular preparation were induced on fracture surfaces.

3. Results and discussion

3.1. Structural evaluation

In the first 5 h of milling, Al particles are deformed into lamellae and weld together, creating secondary particles (Fig. 1a). Upon further milling, the thickness of the lamellae decreases to such an extent that it cannot be distinguished by optical microscopy (Fig. 1b). After 20 h, the morphology changes from plate-like into equiaxed form (Fig. 1c). Comparing Fig. 1c and Fig. 1d (Al milled for 25 h), it seems that the system reached a steady state after 20 h of milling. It must be noted that the layered structure of Al remains after achieving the steady state but it has no preferred orientation (Fig. 1e). Indeed, the laminated initial Al particles are thinner than anything that can be observed by OM [1].

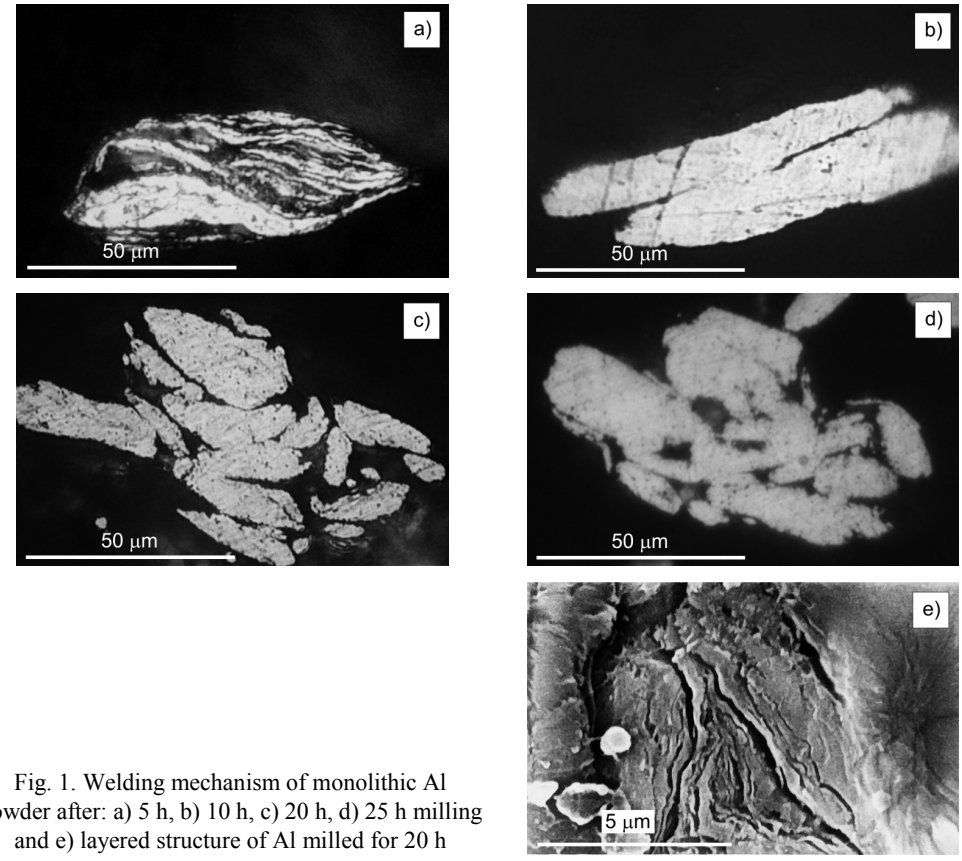

Fig. 1. Welding mechanism of monolithic Al powder after: a) 5 h, b) 10 h, c) 20 h, d) 25 h milling and e) layered structure of Al milled for 20 h

In the case of the Al–Al_2O_3 system, the presence of alumina particles prevents any formation of Al, flake-like particles after 5 h of milling (Fig. 2a). Indeed, before deforming into a flaky shape, Al particles are torn by Al_2O_3 particles and thus, microwelding occurs among spherical, rather than plate-like, particles. Comparing the composite powders milled for 15 h and 20 h (Figs. 2b, c), it is obvious that welding and

fracture have reached a steady state after 15 h milling. High plastic deformation in the vicinity of alumina particles increases the work hardening rate of Al matrix, thus the fracture and welding mechanism achieve equilibrium in a shorter time [4].

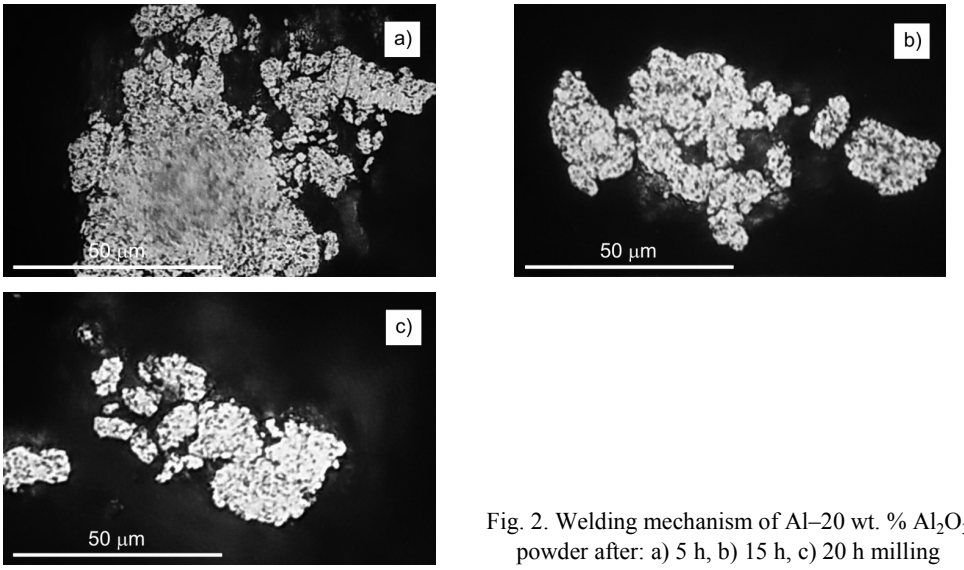

Fig. 2. Welding mechanism of Al–20 wt. % Al_2O_3 powder after: a) 5 h, b) 15 h, c) 20 h milling

Two types of porosity can be distinguished in the milled powder: pores of about 5–10 μm (Fig. 1d) caused by cold welding of the powder and pores existing only in the composite powder, caused by the Al_2O_3 particles penetrating into the Al matrix, resulting in fine pores distributed uniformly among the matrix (Fig. 2b). The formation of any types of pores decreases the apparent density of the powder (Fig. 3). A slight increase in the apparent density of the composite powder after 25 h of milling is attributed to the presence of Fe debris caused by the abrasion of balls and vial, thereby increasing the density of the powder.

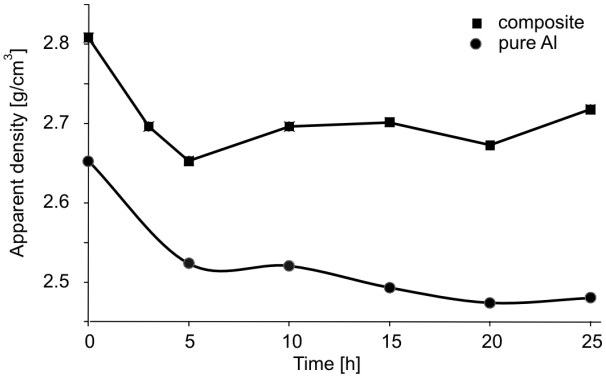

Fig. 3. Time dependence of the apparent density of monolithic and composite powders

Fe content in the monolithic Al powder increases by 0.4% after completion of the milling process (Table 1). Presence of the alumina particles in the composite system increases the abrasion so that Fe amount in the reinforced powder is larger than in monolithic powders (Table 2).

Table 1. The composition of as-received and 25 h milled monolithic Al

Sample	Zn	Ni	Cr	Fe	Ti	Cu	Mn
As received Al [%]	0.021	0.003	<0.004	0.42	0.008	0.0007	<0.01
Milled monolithic Al [%]	0.017	0.092	<0.004	0.87	0.01	0.046	0.128

Table 2. Effect of milling time on the Fe amount of the reinforced powder

Milling time [h]	0	5	10	15	20	26
Fe [%]	0.42	1.49±0.53	1.786±0.35	2.01±0.4	2.48±0.17	2.65±0.47

In order to evaluate the nature of the Fe phase, whether it is in the form of a solid solution or a particulate, the Nelson–Riely method was used to estimate the Al lattice parameter [19]. Results show that the lattice parameter increased immediately after 5 h of milling and then it decreased after further milling, for both the monolithic and the composite powder (Table 3).

Table 3. Effect of milling time on the lattice parameter of Al in the monolithic and composite powder

Milling time [h]	0	5	10	15
Composite powder	4.047	4.048	4.047	4.046
Monolithic powder	4.047	4.049	4.048	4.048

Decomposition of the PCA by a mechanochemical process, followed by solid solution of C and O atoms in the Al lattice, is responsible for the abrupt increase in the first 5 h [21]. Two different mechanisms can be considered for the decrease in the lattice parameter. In the case of pure Al, due to surface tension of grains, the lattice parameter decreases with the grain size reduction [22, 23].

In the case of the composite powder, the lower lattice parameter of Al is ascribed to dissolution of Fe debris into Al [24]. The smaller atomic radius of Fe (0.126 nm) compared with that of Al (0.143 nm) reduced the lattice parameter. However, after the annealing process, the dissolved Fe atoms react with Al to form Fe–Al intermetallic (the needle-like white particles in Fig. 4).

High plastic deformation produces too many imperfections in the Al lattice such as GBs and dislocations. The more imperfections created in the matrix, the more evident peak broadening can be seen in the XRD pattern.

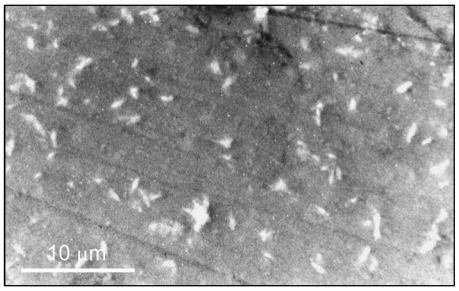

Fig. 4. Al–Fe intermetallic in the annealed composite sample milled for 20 h

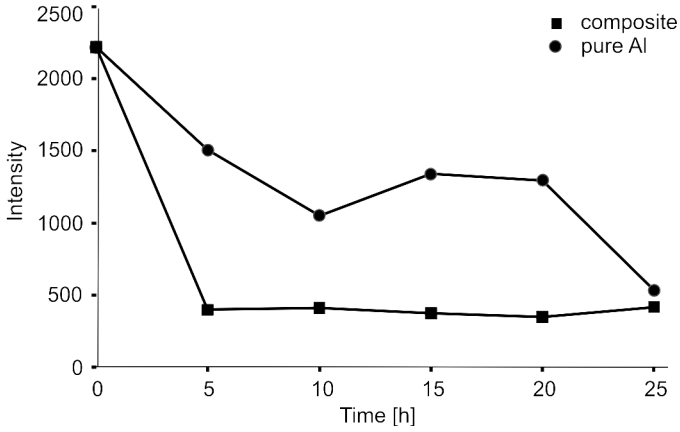

Fig. 5. Dependence of the intensity of the (111) peak of Al for monolithic and composite powders on the milling time

Figure 5 shows that the intensity of the (111) reflection for Al in the composite powder decreases faster compared with the monolithic Al. As mentioned before, the presence of Al_2O_3 particles assists work hardening, thus saturation of imperfection and consequently steady state takes place in a shorter time [4, 25]. For pure Al, it is at least 10 h milling. This can be understood by considering the anisotropy in the elastic module of Al single crystal. Therefore, grains within a powder particle are deformed into thin layers in the 'soft' direction, perpendicular to the direction in which the powder particles were flattened by the milling ball. When the sample is prepared, in order to perform the powder XRD analysis, this flattened powder and its (200) planes are arranged parallel to the sample holder, i.e., I_{200} increases whereas I_{111} decreases [26]. With further milling, the flattened particles are fractured and divided to equiaxial particles. Therefore particles lose their preferred orientation, and their planes of reflection are randomly arranged again and I_{111} recovers its significance. In a different manner, I_{111} of the reinforced Al has an abrupt reduction after 5 h of milling without any considerable change afterwards. This confirms lack of any lamination of the Al particles in the presence of alumina.

3.2. Fractography

As a determinant criterion, prior knowledge of the structural traits is essential for fractography. Grain size estimates for the sintered samples, obtained by XRD, and the Williamson–Hall equation [18] show that in spite of time and temperature, the grains did not grow markedly during heating and had a constant diameter of about 80 nm. The presence of nanometric carbide and oxide particles created by the decomposition of PCA results in the Zener pinning mechanism, and so grain growth ceases [27].

On the other hand, GB energy can be decreased by the accumulation of Fe atoms in the GB region, thus the presence of Fe impurity in the form of solid solution can retard the grain growth mechanism [28, 29]. By migration of the boundaries, the concentration of Fe atoms in the boundary regions increases and thus driving force for boundary migration, i.e. GB energy reduces. Accordingly, grain growth is suppressed at the early stages of annealing [30, 31].

Hardness is inversely proportional to the grain size, according to the Hall–Petch formula (Eq. (3)) [32, 33], thus a fracture surface different from the usual one is anticipated for the milled product samples.

$$H = H_0 + KD^{-1/2} \tag{3}$$

where H_0 is the hardness of the annealed coarse grained sample, K is a constant and D is the size of a crystallite.

In the case of monolithic Al sample (Fig. 6a), microvoid coalescence and hence dimple rupture is known as the main fracture mechanism. In the absence of any inclusion or second phase particles, prior particle boundaries act as the proper sites for nucleation of dimples (Fig. 6b). Such elongated dimples, arranged in the same direction, indicate that the fracture surface results from tear [34].

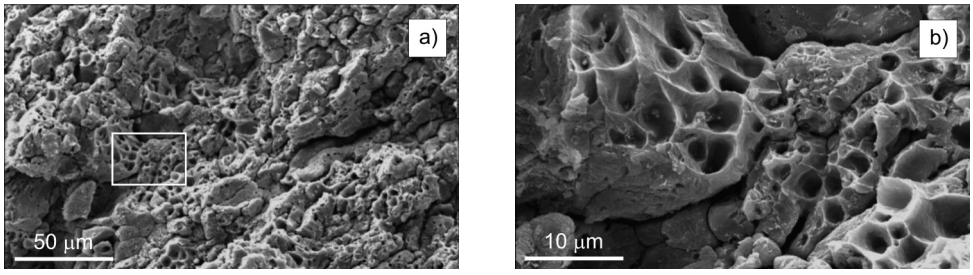

Fig. 6. Fracture surface of monolithic Al without milling

There is a different fracture surface of Al milled for 25 h (Fig. 7a). The fracture surface is covered with microvoids of different shapes compared with one produced by microvoid coalescence (Fig. 7b). Indeed, the presence of the alumina layer on the surface of initial Al particles reduces the cohesive strength of the material at the particle boundaries and promotes decohesive rupture mechanism (Fig. 7c).

On the other hand, due to the presence of a high volume proportion of the GB phase, another suitable region for crack propagation must be considered [17]. In the

nanocrystalline (NC) regime, the spatial confinement of the grains below several tens of nanometres inhibits the operation of dislocation sources inside grains, limiting the plastic deformation [12, 15].

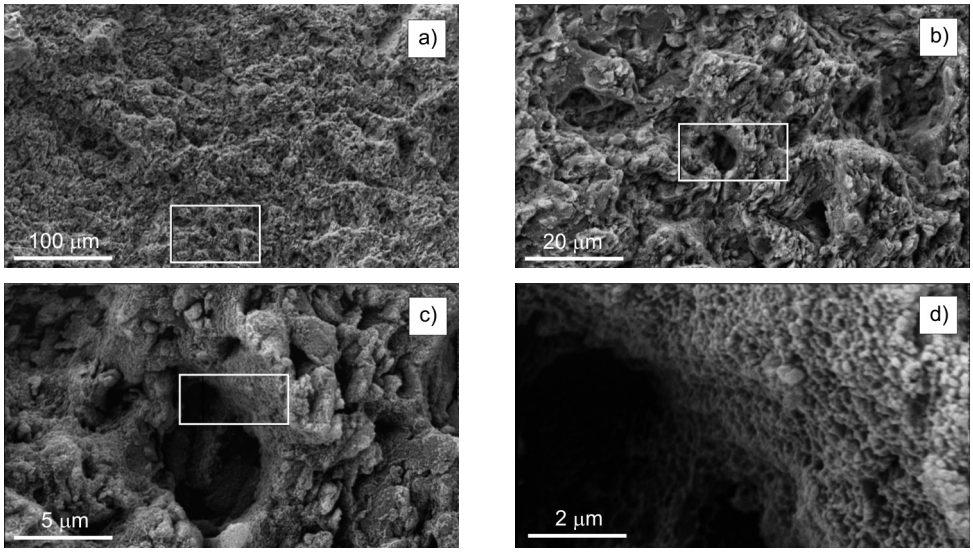

Fig. 7. Fracture surface of monolithic Al milled for 25 h at various magnifications

It is expected that in NC plastic deformation can be accommodated by the GBs. Rotation of grains, together with GB sliding, creates nanometric pores along the GBs acting as thresholds of crack propagation. Since GB shave the lowest melting point of an alloy system and are easy paths for diffusion and sites for segregation, cracks propagate along the GBs and thus an intergranular fracture is anticipated in nanocrystalline materials [16]. Figure 7d shows that creation of dimples proceeded along the GBs, resulting in a different mode of intergranular fracture accompanied by decohesive rupture.

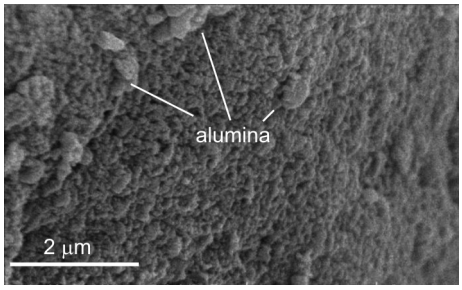

Fig. 8. Fracture surface of composite sample fabricated by 20 h milling

Addition of 20 wt. % of alumina powder has no considerable effect on the fracture surface of milled samples (Fig. 8). Since GBs are more accessible than alumina particles, microvoids tend to propagate along the GBs rather than along the mismatch be-

tween the Al–Al_2O_3 phases. Despite the presence of alumina particles (marked with in the picture), fracture surface is completely intergranular.

4. Conclusion

High energy milling of monolithic Al and Al–20 wt. % Al_2O_3 was studied in terms of its structural evolution. Addition of 20 wt. % of Al_2O_3 to the Al powder changed the cold welding mechanism and hence the preferred orientation and porosity in the Al matrix. The presence of alumina powder caused Fe impurity, which dissolved in the matrix during milling. This changes the Al lattice parameter,and also produces an Al-Fe intermetallic after annealing. In the case of a milled powder, grain boundary sliding and decohesion of initial particles are known to be the two mechanisms that cause fracture, therefore, a combination of intergranular and decohesive rupture is observed in the fracture surface.

References

[1] FOGOGNOLO J.B., VELASCO F., ROBERT M.H., TORRALBA J.M., Mater. Sci. Eng. A, 342 (2003), 131.
[2] RAZAVI HESABI Z., SIMCHI A., SEYED REIHANI S.M., Mater. Sci. Eng. A, 428 (2006), 159.
[3] FOGOGNOLO J.B., ROBERT M.H., TORRALBA J.M., Mater. Sci. Eng. A, 426 (2006), 85.
[4] FOGOGNOLO J.B., RUIZ-NAVAS ELISA M., ROBERT M.H., TORRALBA J.M., Mater. Sci. Eng. A, 355 (2003), 50.
[5] ZEBARJAD S.M., SAJJADI S.A., Mater. Design, 28 (2007), 2113.
[6] RUIZ-NAVAS E.M., FOGAGNOLO J.B., VELASCO F., FROYN L., Composites A, 37 (2006), 2114.
[7] PRABHU B., SURYANARAYANA C., AN L., VAIDYANATHAN R., Mater. Sci. Eng. A, 425 (2006), 192.
[8] RODIGUEZ A., GALLARDO J.M., HERRERA E.J., J. Mater. Sci., 32 (1997), 3535.
[9] SURYANARAYANA C., Prog. Mater. Sci., 46 (2001), 1.
[10] HONGQI L., EBRAHIMI F., Adv. Mater., 17 (2005), 1969.
[11] DALLA TORRE F., VAN SWYGENHOVEN H., VICTORIA M., Acta Mater., 50 (2002), 3957.
[12] KUMAR K.S., SWYGENHOVEN H.V., SURESH S., Acta Mater., 53 (2003), 5743.
[13] MEYERS M.A., MISHRA A., BENSON D.J., Prog. Mater. Sci., 51 (2006), 427.
[14] MUKAIA T., KAWAZOEB M., HIGASHI K., Nanostruct. Mater., 10 (1998), 755.
[15] IWASAKI H., HIGASHI K., NIEH T.G., Scripta Mater., 50 (2004), 395.
[16] LI H., EBRAHIMI F., Acta Mater., 54 (2006), 2877.
[17] HASNAOUI A., VAN SWYGENHOVEN H., DERLET P., Science, 300 (2003), 1550.
[18] WILLIAMSON G.K., HALL W.H., Acta Metal., 1 (1953), 22.
[19] NELSON J.B., RIELY D.P., Proc. Phys. Soc. (London), 57 (1945), 160.
[20] HAROLD P.K., ALEXANDER L.E. *X Ray Diffraction Procedure*, Wiley, New York, 1954.
[21] XIA Z.P., LI Z.Q., LU C.J., ZHANG B., ZHOU Y., J. Alloys Comp., 399 (2005), 139.
[22] KORCHEF A., CHAMPION Y., NJAH N., J. Alloys Comp., 427 (2007), 176.
[23] LIU M., SHI B., GUO J., CAI X., SONG H., Scripta Mater., 49 (2003), 167.
[24] ORTIZ A.L., SHAW L., Acta Mater., 52 (2004), 2185.
[25] FOGOGNOLO J.B., ROBERT M.H., TORRALBA J.M., Mater. Sci. Eng. A, 426 (2006), 85.
[26] AMADOR D.R., TORRALBA J.M., J. Mater. Proc. Tech., 143–144 (2003), 776.
[27] ZENER C., Trans. AIME, 175 (1948), 15.
[28] KIRCHHEIM R., Acta Mater., 50 (2002), 413.

[29] LIU F., KIRCHHEIM R., Acta Mater., 51 (2004), 521.
[30] LIU F., YANG G., KIRCHHEIM R., J. Crystal Growth, 264 (2004), 392.
[31] LIU K.W., MUCKLICH F., Acta Mater., 49 (2001), 395.
[32] HALL E., Proc. Phys. Soc. B, (1951), 747.
[33] PETCH N., J. Iron Steel Inst., 174 (1653), 25.
[34] DAVIS J.R., *Aluminum and Aluminum Alloys*, ASM International, Almere, 1993.

Received 29 July 2008
Revised 7 November 2008